

Experimental Studies on Parametric Effects and Reaction Mechanisms in Electrolytic Decomposition and Ignition of HAN Solutions

Dashan Sun, Qiqiang Dai, Wai Siong Chai, Wenjun Fang, and Hua Meng*



Cite This: *ACS Omega* 2022, 7, 18521–18530



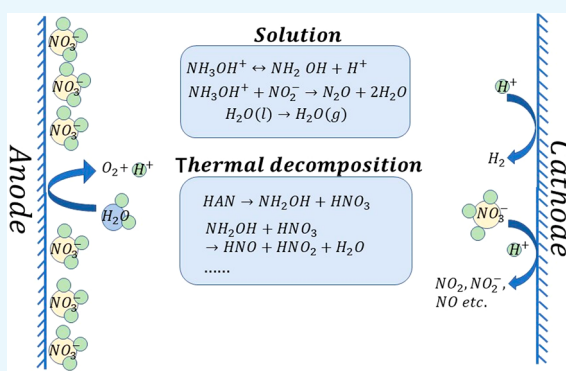
Read Online

ACCESS |

Metrics & More

Article Recommendations

ABSTRACT: The green propellant hydroxylammonium nitrate (HAN) is a good alternative to the conventional propellants in space propulsion applications because of its low toxicity and high energy density. Electrolytic decomposition and ignition of HAN solution, an ionic liquid, is a promising approach. In this work, comprehensive experimental studies were conducted to examine effects of different electrolytic voltages, electrode surface areas, and HAN concentrations on the decomposition process. In the test cases, an optimum electrolytic voltage appears to exist, which leads to the fastest decomposition process. As the voltage increases, a larger electrode surface area on the anode side should be used to overcome an anodic inhibition phenomenon and accelerate the electrolytic process. A high concentration of HAN solution is preferred for its decomposition and ignition. Results also reveal that the electrolytic process of a HAN solution could eventually trigger thermal decomposition reactions, raising the maximum temperature to around 550 K at the final stage. A detailed chemical reaction mechanism was proposed, based on the experimental data and FTIR spectra analyses. Results obtained herein would provide fundamental understandings on the complex electrochemical and physical processes and should be helpful for future applications of the electrolytic decomposition and ignition technology.



1. INTRODUCTION

Energetic ionic liquids are considered as promising alternative propellants in space missions to replace the conventional propellant hydrazine, which is highly toxic and raises serious safety concerns.^{1,2} The most studied ionic liquids for propulsion applications include hydrazinium nitroformate (HNF), hydroxylammonium nitrates (HAN), and ammonium dinitramide (ADN).³ Among them, HAN (its chemical formula is $[\text{NH}_3\text{OH}^+][\text{NO}_3^-]$) has a comparable specific impulse as hydrazine but is environment-friendly, which makes a HAN-based propulsion system safe to handle, suitable for recycling, and cost-effective in space missions.

Thermal and catalytic decomposition are two common approaches for ignition of HAN solutions and its mixtures with fuels. Many studies have been conducted on thermal decomposition of HAN to obtain fundamental understandings on the chemical processes and reaction mechanisms. Oxley and Brower⁴ and Lee and Litzinger⁵ carried out experimental studies on HAN thermal decomposition at atmospheric pressure. The formation of nitrous oxide was reported, and a reduced reaction mechanism was proposed and numerically validated.⁵ Izato et al.^{6,7} and Zhang et al.⁸ applied density functional theory (DFT) to study the basic processes of HAN

thermal decomposition and obtained detailed chemical kinetic models. From these existing studies, it is revealed that the initial reaction in HAN thermal decomposition involves proton transfer from the hydroxylamine ion ($[\text{NH}_3\text{OH}^+]$) to the nitrate ion ($[\text{NO}_3^-]$), which is the rate-determining step with a high activation energy. Therefore, catalytic decomposition of HAN has attracted further research interests.

A variety of catalysts have been applied to efficiently reduce the initiating temperature in thermal decomposition of HAN solutions or HAN-based propellants. Esparza et al.⁹ applied the iridium/rhodium foam particles as catalysts and was able to reduce the initial decomposition temperature of a HAN solution by 60 K. It was concluded that the catalytic effect increases the pre-exponential factor in the reaction mechanism rather than reduces the activation energy. Catalysts consisting of iridium combined with metal oxides have been extensively

Received: February 27, 2022

Accepted: May 6, 2022

Published: May 20, 2022



investigated, including Ir–CuO,^{1,10} Ir–Al₂O₃,¹¹ and Ir–CeCo.^{12,13} Catalysts based on different noble metals have also been tested. For example, Courtheoux et al.^{14–16} used the Pt–Si–Al₂O₃ catalyst and found out that the Pt nanoparticles play a main catalytic role in the decomposition process.

Because of its ionic nature, electrolytic decomposition of HAN solution has been considered as an alternative and efficient approach,^{17–20} with potential advantages of a simple ignition system and effective thermal management in space missions. In electrolytic decomposition of HAN solutions, ignition is achieved by the combined effects of Joule heating, provided by the current, and a reduction of thermal stability of the HAN solution. The magnitude of the current is closely related to the applied voltage, the electrode surface area, and the solution conductivity, while electrode materials could further affect the electrolytic performance by directly influencing the surface chemical reactions. A variety of electrode materials have been tested in electrolytic decomposition of HAN solutions, including titanium,¹⁷ silver,¹⁸ copper,^{21,22} aluminum,²³ and graphite.²⁴ It was indicated that the gaseous products and heat release during the decomposition process would create a strongly oxidizing environment that could consume these electrode materials. It was also revealed that the use of these sacrificial electrodes could accelerate the electrolytic process and accomplish high ignition temperature because the electrode consumption provides additional current while the reaction products, such as nitrogen oxides, decrease the thermal stability of the HAN solution. On the other hand, however, short working time and poor repeatability of the electrodes prevent its engineering applications. As a result, noble metals, such as platinum,²⁵ are generally needed as potential electrode materials in order to achieve good electrolytic performance and sufficient electrode lifespan. In a recent study,²⁶ stainless steel (SS) and platinum (Pt) were tested as a pair of hybrid electrodes and were found to have reliable and repeatable electrolytic performance. In particular, a combination with SS as a cathode and Pt as an anode (the SS–Pt electrodes) was shown to provide the optimum performance.

In this work, a series of experimental studies have been conducted to analyze the electrolytic decomposition and ignition of HAN solutions, using the hybrid SS–Pt electrodes.²⁶ Parametric effects of different electrolytic voltages, electrode surface areas, and HAN solution concentrations on the decomposition process are investigated in detail. Based on the experimental data, results from the Fourier transform infrared (FTIR) spectra of gaseous decomposition products, and results from previous studies, the chemical reaction mechanism is further proposed.

2. EXPERIMENTAL SETUP

HAN was first synthesized by neutralization of the diluted aqueous solution of nitric acid (Sinopharma, China) and hydroxylamine (Adamas, China), based on the detailed procedures presented in a previous work.²⁴ The aqueous HAN solution was then purified using a rotary evaporator under vacuum conditions. Different concentrations of the aqueous HAN solution could then be obtained using the following density method:¹⁶

$$\rho = \frac{107.85}{96.042 - 30.99w(\text{HAN})} \quad (1)$$

The present experiments of HAN electrolysis and ignition were conducted in a sealed glass beaker with an inner diameter of 40 mm and a height of 40 mm, as shown in Figure 1. Four

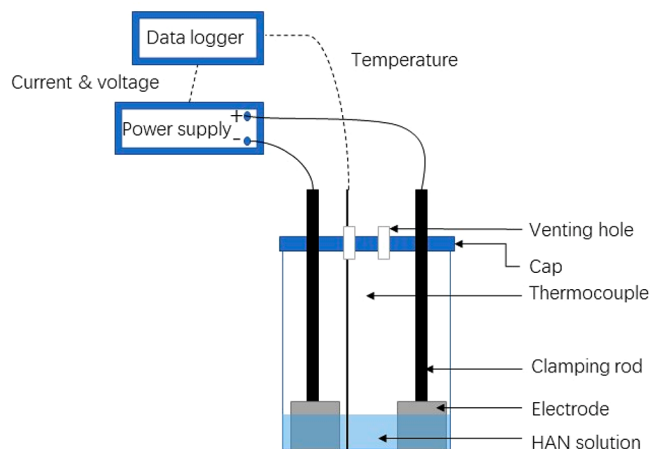


Figure 1. Experimental setup (solid lines represent electric connection, and dotted lines represent data transmission).

holes were drilled in the Teflon seal to insert two electrode clamping rods for current conduction, a thermocouple for temperature measurement, and a venting tube for exhausting gas products and collecting samples for subsequent analyses using FTIR spectroscopy. In the latter case, the venting tube was connected to a gas container. The electrode rods were connected to a DC power supply with a voltage range of 0–60 V, a current range of 0–25 A, and a maximum power of 1500 W. Data were recorded in a data logger at a frequency of 10 Hz.

Prior to each experiment, the glass beaker, electrode clamp rods, and electrodes were all washed with deionized water before HAN solution was added; the electrodes of different widths were properly assembled to maintain a constant depth inside the HAN solution; the thermocouple was immersed in HAN solution to measure its evolution temperature. After each experiment, the circuit was disconnected, and the reaction system was disassembled and cleaned.

3. EXPERIMENTAL RESULTS

In this work, effects of different electrolytic voltages, electrode surface areas, and HAN concentrations (based on 6 g of HAN) on electrolytic decomposition of HAN solutions are experimentally investigated.

3.1. Effect of Electrolytic Voltage. In experimental studies in this section, 80 wt % of HAN solution is used, and the geometric dimensions of SS–Pt electrodes are 10 mm × 10 mm × 0.1 mm in height, width, and thickness (the base electrodes, Pt: 10 mm, SS: 10 mm).

Figure 2a–c shows temporal variations of the temperature and electric current under different voltages, ranging from 20 to 60 V. At a relatively low voltage of 20 V, as shown in Figure 2a, the current first increases, reaching a maximum value of around 2.1 A at 60 s and then gradually decreases, returning to 0 A at 290 s. The measured temperature initially increases and reaches 400 K at 130 s. Afterward, it starts to fluctuate slightly between 390 and 410 K, mainly because of heat loss to the gas products. In this case, the final stage of HAN thermal

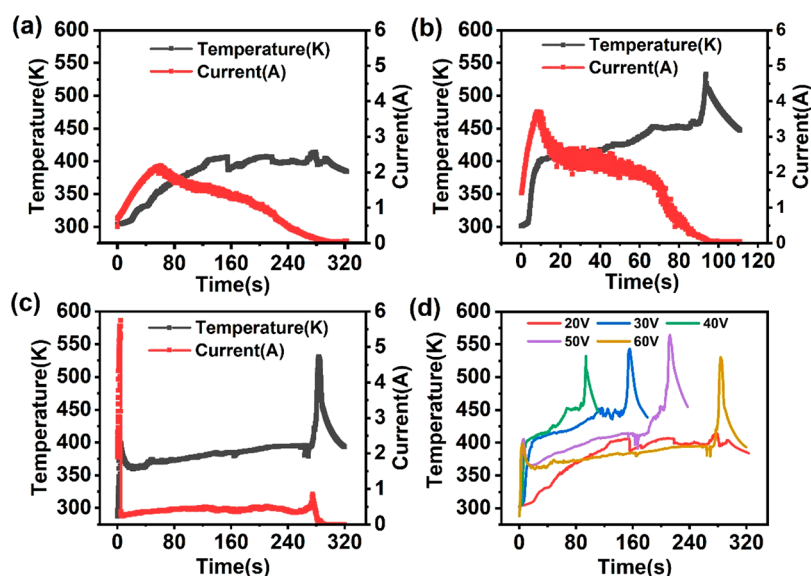


Figure 2. Temporal variations of temperature and current (a) under 20 V, (b) under 40 V, and (c) under 60 V. (d) Temporal variations of temperature under different voltages from 20 to 60 V.

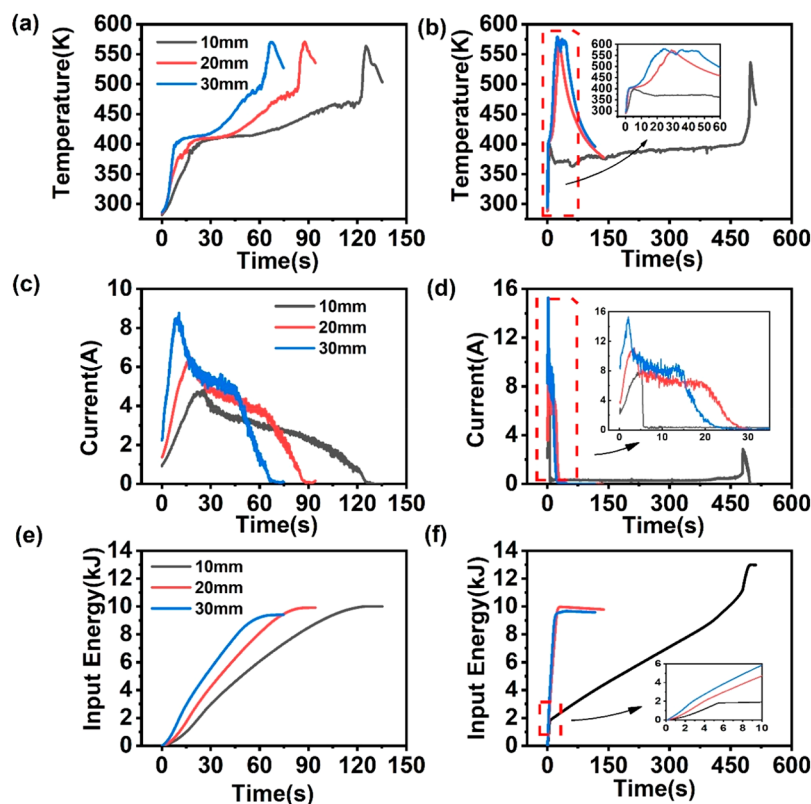


Figure 3. Temporal evolutions of temperature with different electrode widths (10 to 30 mm), (a) under 30 V and (b) under 60 V. Temporal evolutions of current with different electrode widths (10 to 30 mm), (c) under 30 V and (d) under 60 V. Temporal evolutions of input electric energy with different electrode widths (10 to 30 mm), (e) under 30 V and (f) under 60 V.

decomposition, as discussed in section 4, cannot be triggered by the electrolytic process.

Results from electrolytic decomposition of HAN solution at 40 V are presented in Figure 2b. Based on variations of both electric current and temperature, the decomposition process can be divided into three stages. The current rises sharply in a short period from 0 to 10 s (stage I) and then starts to decrease, dropping initially slowly from 20 to 70 s and then

rapidly to reach zero at 95 s (stage II). In stage II, the electric current oscillations can also be observed. The temperature also strongly increases in stage I; its increasing rate then slows down significantly in stage II and finally undergoes a sharp increase again from around 95 s (stage III, at which the electric current remains zero). The peak temperature in stage III can reach around 550 K.

Figure 2c presents the temporal evolutions of current and temperature in an electrolytic decomposition process under 60 V. Both the electric current and temperature increase sharply from 0 to 4.5 s, and then each rapidly drops to and remains at a relatively low but stable value until around 275 s. It appears that the electrolytic decomposition process is strongly suppressed during this period. The current and temperature eventually undergo a second round of sharp increase, particularly for the temperature, which rises and reaches a peak value at around 550 K.

The temporal variations of temperature under different voltages are summarized and compared in Figure 2d. It can be clearly observed that once the voltage becomes higher than 20 V, a peak temperature at around 550 K can be reached for all of the test cases. Moreover, from 20 to 40 V, the time taken to reach peak temperature decreases as the voltage increases. On the other hand, from 40 to 60 V, the time taken to reach peak temperature increases as the voltage increases, due to the inhibition effect at a high voltage, as explained in section 4. Therefore, it appears that an optimum voltage, e.g., at around 40 V, exists for achieving the fastest electrolytic decomposition process. Furthermore, at the voltage of 40 V (the process is similar under a voltage from 30 to 50 V), the electrolytic process can be clearly divided into three stages. In stage I, the temperature rises sharply from room temperature to around 400 K, while the current also rises rapidly. In stage II, the temperature will rise slowly but continuously to around 440 K, while the current will gradually fall to zero, with certain oscillations. In stage III, the temperature rapidly rises again to around 550 K, while the current remains zero. The underlying chemical and physical reasons leading to these phenomena will be analyzed in detail in the following section 4.

3.2. Effect of Electrode Surface Area. In the following experiments, the HAN solution concentration is maintained at 80 wt %. The heights and thicknesses of the two electrodes remain at 10 mm and 0.1 mm, respectively, but the widths of both electrodes vary from 10 to 30 mm to investigate effects of different electrode surface areas on electrolytic decomposition of a HAN solution.

At an electric voltage of 30 V, as shown in Figure 3a,c, experimental results of transient variations of the current and temperature clearly indicate that the increased electrode area would speed up the electrolytic decomposition process in both stages I and II and also increase the maximum current in stage I. Moreover, as the electrode surface area is increased, Figure 3e indicates that the input electric energy rate slightly increases, but the total input energy consumption remains almost the same, e.g., at 10008, 9918, and 9407 J, with 10–30 mm electrodes under 30 V.

Effects of the electrode surface area on HAN electrolytic decomposition are further studied at 60 V, as shown in Figure 3b,d. As presented previously in section 3.1 and in Figure 2c, with the two base electrodes, the electrolytic decomposition process in stage II was strongly suppressed under 60 V and takes a very long time to complete. However, as the electrode surface area is increased, e.g., using two wide electrodes at a width of 20 or 30 mm, the suppressing effect could be drastically relieved, the process in stage II is significantly shortened, and the time to reach peak temperature would be reduced to less than 30 s, as shown in the inset of Figure 3b,d.

Effects of the electrode surface area also lead to differences in the input electric energy rate and total input energy consumption. At 60 V, as the electrode surface area is

increased, the input electric energy rate significantly increases, as shown in Figure 3f, but the total energy consumption decreases, e.g., from 12982 to 9781 J, with the electrode width changed from 10 to 20 mm (the effect becomes minor as the electrode width further increases to 30 mm). The difference in total energy consumption is believed to be related to heat loss to the outside environment during an experiment, which is larger in a longer process.

In summary, it appears that the electrode surface areas play a very important role in accelerating the electrolytic process of HAN solutions, particularly for the case at a high electrolytic voltage of 60 V. In this case, drastic changes occur, particularly when the two electrode widths are increased from 10 to 20 mm.

Separate effects of the anode and cathode electrode surface areas on the electrolytic decomposition of HAN solutions are further examined, using different combinations of the anode and cathode electrodes with two different widths of 10 and 20 mm.

Figure 4 shows the effects of different combinations of cathode and anode electrode areas (widths) on HAN

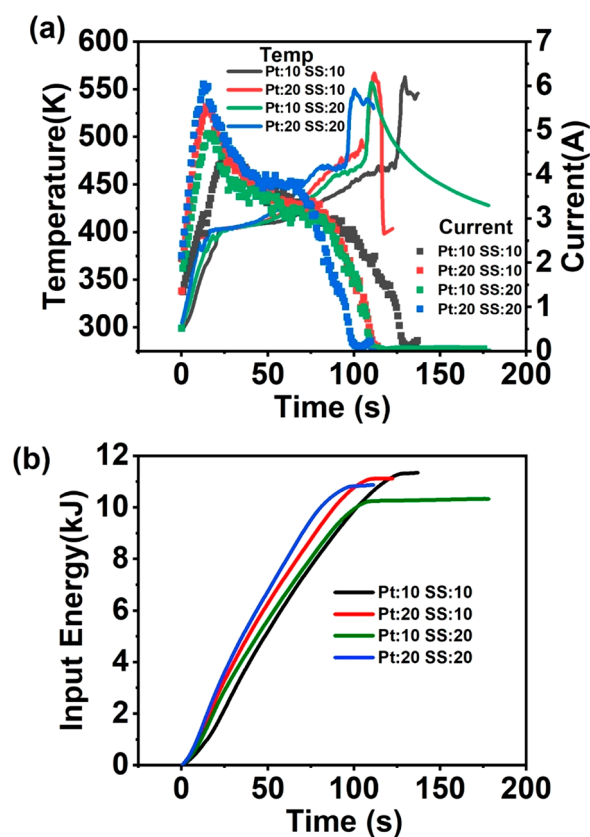


Figure 4. (a) Temporal variations of temperature and current and (b) temporal variations of input electric energy, using different combinations of anode and cathode electrodes with two different widths under 30 V.

electrolytic decomposition at 30 V. In these cases, it appears that an accelerated decomposition rate could be achieved by increasing either the anode (Pt) or cathode (SS) electrode surface area (the electrode width changes from 10 to 20 mm), and it is slightly better to increase only the anode (Pt) electrode area.

Figure 5a presents temporal variations of temperature and current with different combinations of anode and cathode

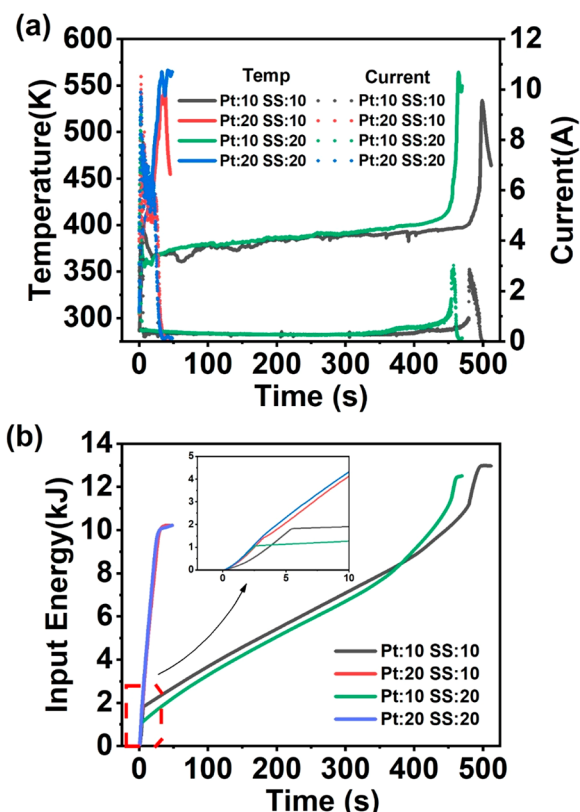


Figure 5. (a) Temporal variations of temperature and current and (b) temporal variations of input electric energy, using different combinations of anode and cathode electrodes with two different widths under 60 V.

electrode areas (widths) under 60 V. Results reveal that the electrolytic process can only be slightly accelerated by increasing the cathode (SS) electrode area, with the total reaction time reduced from around 499 s in the base case (Pt: 10 mm, SS: 10 mm) to around 464 s in the new case (Pt: 10 mm, SS: 20 mm). However, the electrolytic process is significantly accelerated by just increasing the anode (Pt) electrode area (Pt: 20 mm, SS: 10 mm), with the entire electrolytic process drastically shortened to around 37 s in this case. The electrolytic performance can be slightly increased by further increasing the cathode electrode area (Pt: 20 mm, SS: 20 mm). Therefore, experimental results clearly indicate that the anode (Pt) electrode area plays a dictating role in the electrolytic decomposition of HAN solutions. A large Pt electrode is thus recommended for practical applications. It has to be emphasized that an upper limit exists for increasing the electrode area to accelerate the reactions (e.g., an electrode width of 20 mm at 60 V), as shown in Figure 3c,d.

In terms of the electric energy consumption, results in Figures 4b and 5b are consistent with the preceding discussions. For example, Figure 5b clearly reveals that, at 60 V, the case using base electrodes (Pt: 10 mm, SS: 10 mm) shows a longer process and consumes more energy than the cases with a wider anode electrode (e.g., Pt: 20 mm, SS: 10 mm).

3.3. Effect of HAN Solution Concentration. In the following experiments, surface areas of the SS–Pt electrodes

remain the same as those used in section 3.1 (the base electrodes).

Figure 6 shows temporal variations of the temperature and current in electrolytic decomposition of HAN solutions at a

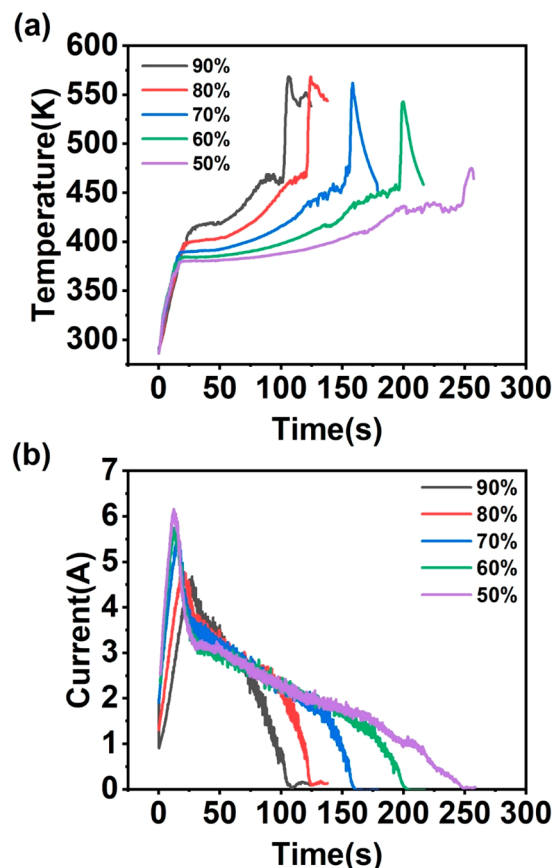


Figure 6. Temporal variations of (a) temperature and (b) current with different HAN concentrations (from 50 to 90%) under 30 V.

voltage of 30 V, with different HAN solution concentrations ranging from 50 to 90 wt %. It can be clearly observed that different HAN concentrations would not affect the temperature increasing rate in stage I, but an increased HAN concentration slightly raises the maximum temperature in this stage. On the other hand, the current rising rate and the maximum current both decrease with an increased HAN concentration. In stage II, as the HAN concentration increases, the temperature rises faster, while the current decreases more rapidly. Overall, the duration of stage II shortens as the HAN concentration increases. In stage III, except for the case with a 50 wt % HAN solution concentration, the temperature can reach a peak value at around 550 K, caused by the final thermal decomposition reactions, as analyzed in the next section.

The measured temperature variations at 60 V, using different HAN concentrations, are presented in Figure 7. Similarly, the decomposition process can be expedited with an increased HAN solution concentration, particularly from 80 to 90 wt %. Moreover, a HAN solution concentration higher than 60 wt % is needed to make stage III accomplishable at 60 V.

4. RESULT ANALYSES AND REACTION MECHANISMS

The experimental results from electrolytic decomposition of HAN solutions are analyzed in this section to obtain

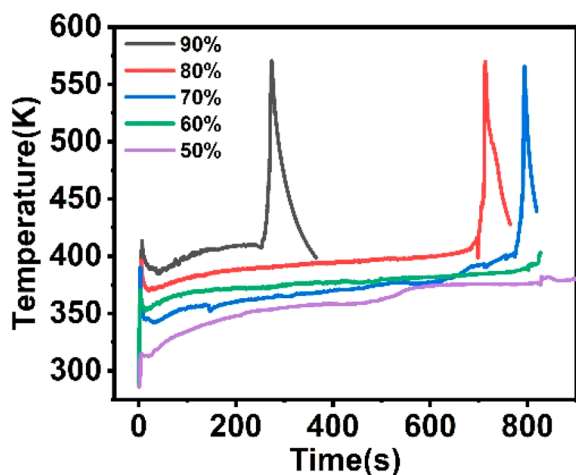


Figure 7. Temporal variations of temperature with different HAN concentrations under 60 V.

fundamental understandings on the electrochemical and physical processes. As presented in section 3, the electrolytic process behaves differently at different voltages. Using the base SS–Pt electrodes (Pt: 10 mm, SS: 10 mm), at an electrolytic voltage of 20 V, the peak temperature is below 410 K in the

entire process (the thermal decomposition reactions cannot be triggered in this case as further discussed), while at 30 and 60 V, the peak temperature can both reach around 550 K, caused by the final thermal decomposition reactions. The decomposition process is relatively fast at 30 V and slow at 60 V, as shown in Figure 3c,d. These two modes are referred to as the “fast mode” and “slow mode” in the following analyses. The characteristics in these two modes at different stages of the decomposition processes are illustrated in Figure 8.

The electrolytic decomposition processes in both fast and slow modes can be divided into three stages, as shown in Figure 8a,b. In stage I, the current can reach a maximum value in a short period of time, while the temperature also increases rapidly. In this stage, gas bubbles start to form on the electrodes and emerge on the liquid surface near the electrodes, as shown in Figure 8a at position 1 in the fast mode and Figure 8b at position 5 in the slow mode. In stage II, the current starts to decrease, generally with oscillations, while the temperature increases gradually. In the fast mode, a large amount of gas bubbles are produced and cover the entire liquid surface, as shown in Figure 8a at position 2. In the slow mode, the process is more complicated. The decomposition process is initially very weak and lasts quite a long time, as shown in Figure 8b at position 6. The slow process is followed by a sudden jump of both current (which then drops very quickly)

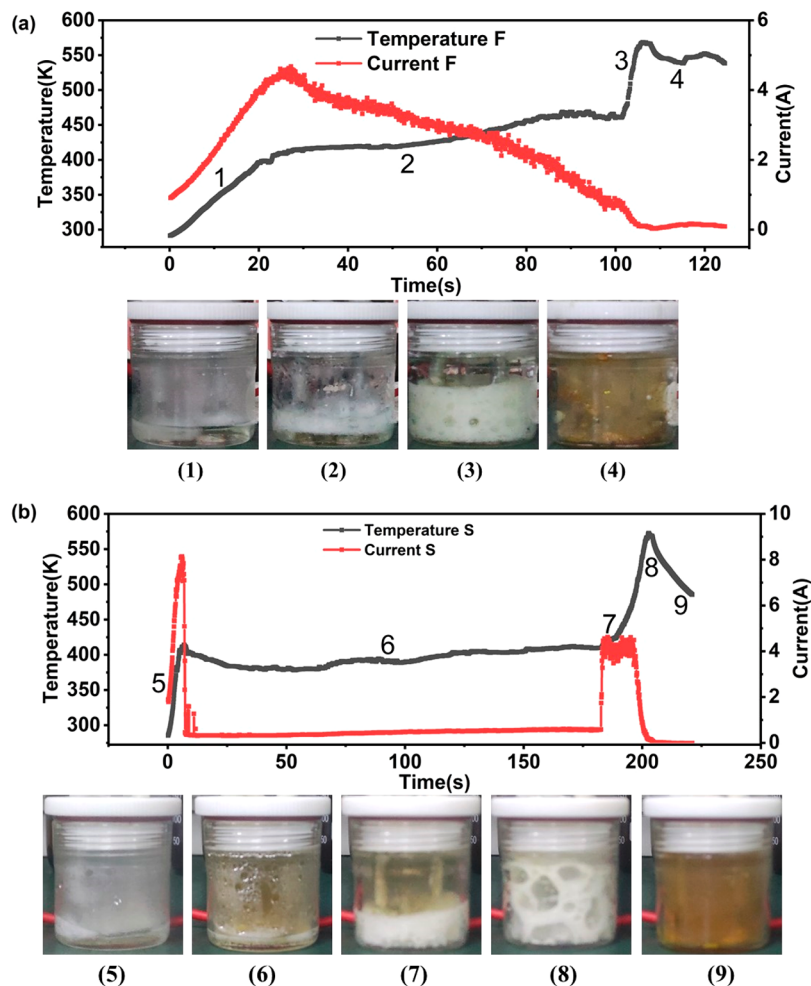


Figure 8. General temporal variations of temperature and current and characteristics of HAN decomposition at different stages in (a) fast and (b) slow modes (1–4 belong to the fast mode and 5–9 to the slow mode).

and temperature, as shown and Figure 8b at position 7. In stage II, electrical sparks can also be observed on the anode side. In stage III, as the temperature of the HAN solution reaches around 440 K, the thermal decomposition process is triggered, resulting in strong expansion of the HAN solution and a large amount of gas bubbles, as shown in Figure 8a at position 3 and Figure 8b at position 8 in the two modes. The final states of complete HAN decomposition are shown in Figure 8a at position 4 and Figure 8b at position 9.

The gas products and HAN solutions are both collected and analyzed. Figure 9 shows the FTIR spectra of the gaseous

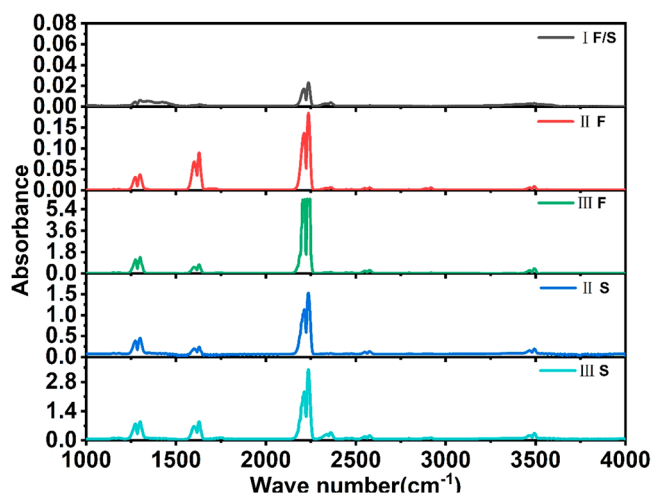


Figure 9. FTIR spectra of the gas products at different stages and in different modes of HAN electrolytic decomposition (F means fast mode, S means slow mode, F/S means both modes; I, II, or III represents the reaction stage in which the sample was taken).

products at different stages in different modes of HAN electrolytic decomposition. It is determined that, at different stages, the gas products contain mainly nitrogen dioxide (NO_2) and nitrous oxide (N_2O), with their characteristic IR absorption peaks at 1630 and 2237 cm^{-1} , respectively²⁷ (the two peaks around 1300 cm^{-1} also correspond to the vibration frequencies of N_2O in these cases).

The spectra of HAN solutions are provided in Figure 10. A HAN solution contains a large amount of NH_3OH^+ and NO_3^- ions. The IR vibration frequencies of NH_3OH^+ are at 1007, 1193, 1520, 1762, 2737, 2984, and 3161 cm^{-1} , the IR frequencies of NO_3^- are at 1040, 1339, and 1393 cm^{-1} , and those of H_2O are at 1613, 3416, and 3569 cm^{-1} .^{24,28} It can be concluded from Figure 10 that the main components of the HAN solution do not change in stages I and II prior to thermal decomposition.

Based on the present experimental observations, FTIR spectra analyses, and previous studies,^{5,19,20} the reaction mechanism of HAN electrolytic decomposition, using the SS–Pt hybrid electrodes, is proposed.

In stage I, as the electrolytic voltage is suddenly enforced, ions in the HAN solution, including mainly NO_3^- , NH_3OH^+ , and H^+ , are quickly attracted to the opposite electrodes and lead to electrochemical reactions, including the redox reactions occurring on both the cathode and anode sides in a very short early period. These processes thereby cause rapid increases of the current and temperature in this stage. The oxygen evolution reaction, which is a four-electron-transfer reaction in an acidic environment,^{29,30} occurs on the anode electrode,

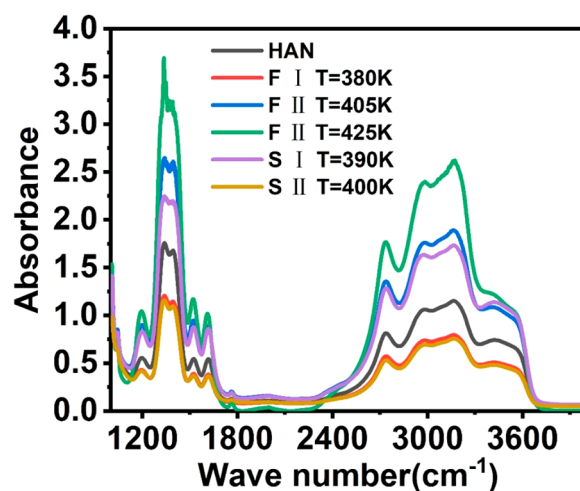


Figure 10. FTIR spectra of the solution at different stages and in different modes of HAN electrolytic decomposition (F means fast mode, S means slow mode, I or II represents the reaction stage in which the sample was taken).

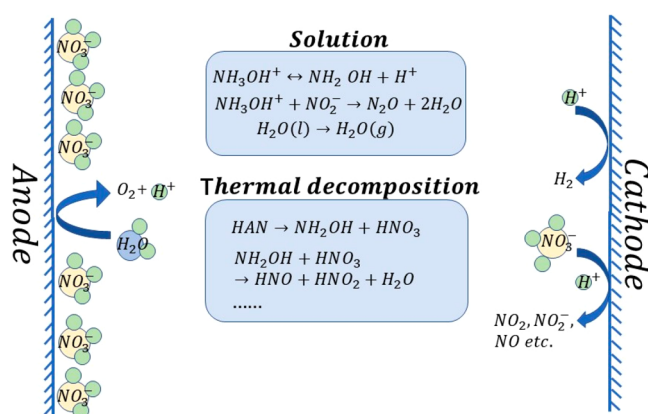
while the hydrogen evolution reaction and the reduction of nitrate ion occur on the cathode electrode. As the HAN solution is weakly acidic (the pH is around 1.65 with a 50 wt % HAN solution), direct reduction reactions of the nitrate ion are considered as the proper reaction mechanism.^{31–34} It should be noted that, because of the present experimental limitations, the quantitative contributions from the two reaction pathways on the cathode side are still unable to be distinguished. The gas products from the electrochemical reactions emerge as gas bubbles from the two electrodes. In the solution, the NH_3OH^+ ion could provide a large amount of H^+ , and reactions between NH_3OH^+ and NO_2^- ions produce N_2O . The detailed chemical reactions are summarized in Table 1.

In stage II, as the cathodic reduction reactions proceed, more NO_2 is produced, with more N_2O from the subsequent solution reaction, as evidenced in Figure 9. As temperature increases, liquid water is strongly evaporated, producing a large amount of gas bubbles and causing current oscillations. However, as the NO_3^- ions cover up the anode electrode surface, as illustrated in Figure 11, the anodic oxygen evolution reaction and correspondingly the cathodic hydrogen evolution reaction are slowed down, leading to the decreased current. At a high electrolytic voltage of 60 V, more NO_3^- ions are attracted to the anode electrode and cover up a large fraction of the electrode surface, leading to a very slow second stage. As NO_3^- ions are gradually consumed, the electrochemical reactions would eventually be accelerated, resulting in a sudden jump of the current and temperature. This could also explain the strong effect of the anode electrode surface area on the electrolytic rate at 60 V. In fact, the inhibition effect with NO_3^- ions covering up the anode electrode also exists in stage I, which leads to the reduced current increasing rate and maximum current in a more concentrated HAN solution, as shown in Figure 6b.

In stage III, as the temperature increases to around 440 K and with more NO_2^- ion produced from the reduction reactions of nitrate ion in stage II, thermal decomposition of HAN is finally triggered. The temperature quickly rises to around 550 K. The related thermal decomposition reaction mechanisms can be found in the literature.^{5–8}

Table 1. Chemical Reaction Mechanism

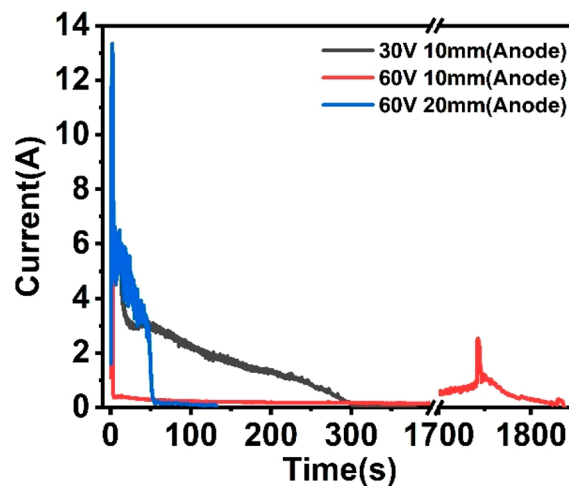
stage	reaction
I	anode: oxygen evolution reaction: $2\text{H}_2\text{O} \rightarrow \text{O}_2 + 4\text{H}^+ + 4\text{e}^-$
	cathode: hydrogen evolution reaction: $2\text{H}^+ + 2\text{e}^- \rightarrow \text{H}_2$
	reduction of nitrate ion: $\text{NO}_3^- + 2\text{H}^+ + 2\text{e}^- \rightarrow \text{NO}_2^- + \text{H}_2\text{O}$
	$\text{NO}_3^- + 2\text{H}^+ + \text{e}^- \rightarrow \text{NO}_2 + \text{H}_2\text{O}$
	solution: $\text{NH}_3\text{OH}^+ \leftrightarrow \text{NH}_2\text{OH} + \text{H}^+$
	$\text{NO}_2^- + \text{NH}_3\text{OH}^+ \rightarrow \text{N}_2\text{O} + 2\text{H}_2\text{O}$
	anode: oxygen evolution reaction: $2\text{H}_2\text{O} \rightarrow \text{O}_2 + 4\text{H}^+ + 4\text{e}^-$
	cathode: hydrogen evolution reaction: $2\text{H}^+ + 2\text{e}^- \rightarrow \text{H}_2$
	reduction of nitrate ion: $\text{NO}_3^- + 2\text{H}^+ + 2\text{e}^- \rightarrow \text{NO}_2^- + \text{H}_2\text{O}$
	$\text{NO}_3^- + 2\text{H}^+ + \text{e}^- \rightarrow \text{NO}_2 + \text{H}_2\text{O}$
II	$\text{NO}_3^- + 4\text{H}^+ + 3\text{e}^- \rightarrow \text{NO} + \text{H}_2\text{O}$
	solution: $\text{NO}_2^- + \text{NH}_3\text{OH}^+ \rightarrow \text{N}_2\text{O} + 2\text{H}_2\text{O}$
	$\text{NH}_3\text{OH}^+ \leftrightarrow \text{NH}_2\text{OH} + \text{H}^+$
	$\text{H}_2\text{O}(\text{l}) \rightarrow \text{H}_2\text{O}(\text{g})$
	HAN thermal decomposition: $\text{HAN} \rightarrow \text{NH}_2\text{OH} + \text{HNO}_3$
	$\text{NH}_2\text{OH} + \text{HNO}_3 \rightarrow \text{HNO} + \text{HNO}_2 + \text{H}_2\text{O}$
III

**Figure 11.** Illustration of the proposed mechanism of HAN electrolytic decomposition.

The proposed chemical reaction mechanism is summarized in Table 1 and illustrated in Figure 11.

In stages I and II, the oxygen evolution reaction is hindered by a large amount of nitrate ions competing for adsorption sites on the anode electrode. This can be further verified by

electrolysis of a simple solution containing NO_3^- , Na^+ , K^+ , and H^+ ions. In this solution, the NO_3^- concentration is 5.37 mol/L, the pH is 1.91, and the Na^+ and K^+ ions play a role in the charge balance. It has the same concentrations of H^+ and NO_3^- ions in this solution as those in a 40 wt % HAN solution. Experiments were conducted at 30 and 60 V using electrodes with different surface areas. As presented in Figure 12, this

**Figure 12.** Temporal evolutions of current in electrolysis of an aqueous solution containing Na^+ , K^+ , H^+ , and NO_3^- using electrodes with different widths under 30 and 60 V.

simple aqueous solution is electrolyzed in the fast mode under 30 V and in the slow mode under 60 V, using a pair of base electrodes. The electrolysis process under 60 V can be significantly accelerated by increasing the anode electrode width to 20 mm. Results obtained with this simple solution appear to confirm the proposed inhibition mechanism in electrolytic decomposition of a HAN solution.

5. CONCLUSIONS

Hydroxylammonium nitrate is a promising green propellant in space propulsion applications. Its solution shows an ionic nature and can thus be decomposed and ignited by an electrolytic process. A series of experimental studies are conducted to examine parametric effects of the electrolytic voltage, electrode surface area, and solution concentration on the electrolytic decomposition and ignition of HAN solutions, using a pair of hybrid electrodes with stainless steel as cathode and platinum as anode. FTIR spectra analyses of the gas products and liquid solutions have also been carried out in this paper. Based on the present experimental observations, FTIR spectra analyses, and previous studies, a detailed reaction mechanism for HAN electrolytic decomposition has been proposed. The main conclusions are summarized in the following:

1. Under proper conditions, an electrolytic decomposition process can generally be divided into three stages. The electrochemical and solution reactions occur in the first two stages. As temperature rises to around 440 K and the concentration of a precursor ion, NO_2^- , increases, HAN thermal decomposition is further triggered in the third stage, which leads to a strong temperature increase to around 550 K at the end of the decomposition process.

- The electrolytic voltage plays a very important role in decomposition and ignition of a HAN solution. With all other conditions fixed, it appears that there exists an optimum voltage, e.g., 40 V in the base cases, that can lead to the fastest decomposition process.
- At a high electrolytic voltage, e.g., 60 V, the decomposition process could become slow and last for a long period of time, caused by an inhibition phenomenon on the anode side. The inhibition effect results in an increased electric energy consumption due to heat loss. This effect can be drastically relieved by increasing the anodic electrode surface area.
- Increasing HAN solution concentration can speed up the electrolytic decomposition process. Therefore, it appears that a HAN solution with high concentration is preferred as long as it is stable in storage.

AUTHOR INFORMATION

Corresponding Author

Hua Meng – School of Aeronautics and Astronautics, Zhejiang University, Hangzhou, Zhejiang 310027, China;
orcid.org/0000-0001-7692-9025; Email: menghua@zju.edu.cn

Authors

Dashan Sun – School of Aeronautics and Astronautics, Zhejiang University, Hangzhou, Zhejiang 310027, China;
orcid.org/0000-0002-1895-1731

Qiqiang Dai – School of Aeronautics and Astronautics, Zhejiang University, Hangzhou, Zhejiang 310027, China

Wai Siong Chai – School of Mechanical Engineering and Automation, Harbin Institute of Technology, Shenzhen, Guangdong 518055, China

Wenjun Fang – Department of Chemistry, Zhejiang University, Hangzhou, Zhejiang 310058, China;
orcid.org/0000-0002-5610-1623

Complete contact information is available at:
<https://pubs.acs.org/10.1021/acsomega.2c01183>

Notes

The authors declare no competing financial interest.

ACKNOWLEDGMENTS

This work was supported by the National Natural Science Foundation of China (12072321).

REFERENCES

- Amrousse, R.; Katsumi, T.; Itouyama, N.; Azuma, N.; Kagawa, H.; Hatai, K.; Ikeda, H.; Hori, K. New HAN-based mixtures for reaction control system and low toxic spacecraft propulsion subsystem: Thermal decomposition and possible thruster applications. *Combust. Flame* **2015**, *162*, 2686–2692.
- Lemmer, K. Propulsion for CubeSats. *Acta Astronaut.* **2017**, *134*, 231–243.
- Gohardani, A. S.; Stanojev, J.; Demairé, A.; Anflo, K.; Persson, M.; Wingborg, N.; Nilsson, C. Green space propulsion: Opportunities and prospects. *Prog. Aeronaut. Sci.* **2014**, *71*, 128–149.
- Oxley, J. C.; Brower, K. R. Thermal decomposition of hydroxylamine nitrate. *Proceeding Society of Photo-Optical Instrumentation Engineers (SPIE)* **1988**, *872*, 63–70.
- Lee, H.; Litzinger, T. A. Chemical kinetic study of HAN decomposition. *Combust. Flame* **2003**, *135*, 151–169.

(6) Izato, Y.; Shiota, K.; Miyake, A. A detailed kinetics model for the decomposition of aqueous hydroxylammonium nitrate. *Sci. Technol. Energy Mater.* **2019**, *80*, 212–221.

(7) Izato, Y.; Koshi, M.; Miyake, A. Decomposition pathways for aqueous hydroxylammonium nitrate solutions: a DFT study. *Cent. Eur. J. Energy Mater.* **2017**, *14*, 888–916.

(8) Zhang, K. Q.; Thynell, S. T. Thermal decomposition mechanism of aqueous hydroxylammonium nitrate (HAN): Molecular simulation and kinetic modeling. *J. Phys. Chem. A* **2018**, *122*, 8086–8100.

(9) Esparza, A. A.; Ferguson, R. E.; Choudhuri, A.; Love, N. D.; Shafirovich, E. Thermoanalytical studies on the thermal and catalytic decomposition of aqueous hydroxylammonium nitrate solution. *Combust. Flame* **2018**, *193*, 417–423.

(10) Amrousse, R.; Katsumi, T.; Azuma, N.; Hori, K. Hydroxylammonium nitrate (HAN)-based green propellant as alternative energy resource for potential hydrazine substitution: From lab scale to pilot plant scale-up. *Combust. Flame* **2017**, *176*, 334–348.

(11) Hwang, C. H.; Baek, S. W.; Cho, S. J. Experimental investigation of decomposition and evaporation characteristics of HAN-based monopropellants. *Combust. Flame* **2014**, *161*, 1109–1116.

(12) Agnihotri, R.; Oommen, C. Cerium oxide based active catalyst for hydroxylammonium nitrate (HAN) fueled monopropellant thrusters. *RSC Adv.* **2018**, *8*, 22293–22302.

(13) Agnihotri, R.; Oommen, C. Evaluation of hydroxylammonium nitrate (HAN) decomposition using bifunctional catalyst for thruster application. *Mol. Catal.* **2020**, *486*, 110851.

(14) Courtheoux, L.; Popa, F.; Gautron, E.; Rossignol, S.; Kappenstein, C. Platinum supported on doped alumina catalysts for propulsion applications. Xerogels versus aerogels. *J. Non-Cryst. Solids* **2004**, *350*, 113–119.

(15) Courtheoux, L.; Gautron, E.; Rossignol, S.; Kappenstein, C. Transformation of platinum supported on silicon-doped alumina during the catalytic decomposition of energetic ionic liquid. *J. Catal.* **2005**, *232*, 10–18.

(16) Courthéoux, L.; Amariei, D.; Rossignol, S.; Kappenstein, C. Thermal and catalytic decomposition of HNF and HAN liquid ionic as propellants. *Appl. Catal., B* **2006**, *62*, 217–225.

(17) Risha, G. A.; Yetter, R. A.; Yang, V. Electrolytic-Induced Decomposition and Ignition of HAN-based Liquid Monopropellants. *Int. J. Energy Mater. Chem. Propul.* **2007**, *6*, 575–588.

(18) Wu, M.-H.; Yetter, R. A. A novel electrolytic ignition monopropellant microthruster based on low temperature co-fired ceramic tape technology. *Lab Chip* **2009**, *9*, 910–916.

(19) Khare, P.; Yang, V.; Meng, H.; Risha, G. A.; Yetter, R. A. Thermal and Electrolytic Decomposition and Ignition of HAN–Water Solutions. *Combust. Sci. Technol.* **2015**, *187*, 1065–1078.

(20) Meng, H.; Khare, P.; Risha, G.; Yetter, R.; Yang, V. Decomposition and ignition of HAN-based monopropellants by electrolysis. In *47th AIAA aerospace sciences meeting including the new horizons forum and aerospace exposition*, 2009, AIAA 2009-451.

(21) Chai, W. S.; Cheah, K. H.; Koh, K. S.; Chin, J.; Chik, T. F. W. K. Parametric studies of electrolytic decomposition of hydroxylammonium nitrate (HAN) energetic ionic liquid in microreactor using image processing technique. *Chem. Eng. J.* **2016**, *296*, 19–27.

(22) Chai, W. S.; Chin, J.; Cheah, K. H.; Koh, K. S.; Ku Chik, T. F. W. Calorimetric study on electrolytic decomposition of hydroxylammonium nitrate (HAN) ternary mixtures. *Acta Astronaut.* **2019**, *162*, 66–71.

(23) Koh, K. S.; Chin, J.; Wahida Ku Chik, T. F. Role of electrodes in ambient electrolytic decomposition of hydroxylammonium nitrate (HAN) solutions. *Propuls. Power Res.* **2013**, *2*, 194–200.

(24) Chai, W. S.; Cheah, K. H.; Meng, H.; Li, G. Experimental and analytical study on electrolytic decomposition of HAN-water solution using graphite electrodes. *J. Mol. Liq.* **2019**, *293*, 111496.

(25) Feess, H.; Köster, K.; Schütz, G. H. The influence of noble metal catalysts on the electro-chemical decomposition of concentrated hydrobromic acid at graphite electrodes. *Int. J. Hydrogen Energy* **1981**, *6*, 377–388.

(26) Chai, W. S.; Sun, D.; Cheah, K. H.; Li, G.; Meng, H. Co-Electrolysis-Assisted Decomposition of Hydroxylammonium Nitrate–Fuel Mixtures Using Stainless Steel–Platinum Electrodes. *ACS Omega* **2020**, *5*, 19525–19532.

(27) Agnihotri, R.; Oommen, C. Kinetics and Mechanism of Thermal and Catalytic Decomposition of Hydroxylammonium Nitrate (HAN) Monopropellant. *Propellants, Explos., Pyrotech.* **2021**, *46*, 286–298.

(28) Amrousse, R.; Katsumi, T.; Sulaiman, T.; Das, B. R.; Kumagai, H.; Maeda, K. Hydroxylammonium nitrate as green propellant: Decomposition and stability. *Int. J. Energy Mater. Chem. Propul.* **2012**, *11*, 241–257.

(29) Park, S.; Shao, Y.; Liu, J.; Wang, Y. Oxygen electrocatalysts for water electrolyzers and reversible fuel cells: status and perspective. *Energy Environ. Sci.* **2012**, *5*, 9331–9344.

(30) Lim, J.; Yang, S.; Kim, C.; Roh, C.-W.; Kwon, Y.; Kim, Y.-T.; Lee, H. Shaped Ir–Ni bimetallic nanoparticles for minimizing Ir utilization in oxygen evolution reaction. *Chem. Commun.* **2016**, *52*, 5641–5644.

(31) Rutten, O. W. J. S.; Sandwijk, A. V.; Weert, G. V. The electrochemical reduction of nitrate in acidic nitrate solutions. *J. Appl. Electrochem.* **1999**, *29*, 87–92.

(32) Wang, Y.; Wang, C.; Li, M.; Yu, Y.; Zhang, B. Nitrate electroreduction: mechanism insight, in situ characterization, performance evaluation, and challenges. *Chem. Soc. Rev.* **2021**, *50*, 6720–6733.

(33) de Groot, M. T.; Koper, M. T. M. The influence of nitrate concentration and acidity on the electrocatalytic reduction of nitrate on platinum. *J. Electroanal. Chem.* **2004**, *562*, 81–94.

(34) Mallika, C.; Keerthika, B.; Mudali, U. K. Platinum-modified titanium anodes for the electrolytic destruction of nitric acid. *Electrochim. Acta* **2007**, *52*, 6656–6664.